Generation of thermofield double states and critical ground states with a quantum computer

D. Zhu[a,b,c], S. Johri[d], N. M. Linke[a,b], K. A. Landsman[a,b], C. Huerta Alderete[a,b,e], N. H. Nguyen[a,b], A. Y. Matsuura[d], T. H. Hsieh[f], and C. Monroe[a,b,c,g,1]

[a]Joint Quantum Institute, University of Maryland, College Park, MD 20742; [b]Department of Physics, University of Maryland, College Park, MD 20742; [c]Department of Electrical and Computer Engineering, University of Maryland, College Park, MD 20742; [d]Intel Labs, Intel Corporation, Hillsboro, OR 97124; [e]Óptica y Electrónica, Instituto Nacional de Astrofísica, Puebla 72840, Mexico; [f]Perimeter Institute for Theoretical Physics, Waterloo, ON N2L 2Y5, Canada; and [g]Joint Center for Quantum Information and Computer Science, University of Maryland, College Park, MD 20742

Contributed by Christopher Monroe, July 29, 2020 (sent for review April 7, 2020; reviewed by David Hayes and Monika Schleier-Smith)

Finite-temperature phases of many-body quantum systems are fundamental to phenomena ranging from condensed-matter physics to cosmology, yet they are generally difficult to simulate. Using an ion trap quantum computer and protocols motivated by the quantum approximate optimization algorithm (QAOA), we generate nontrivial thermal quantum states of the transverse-field Ising model (TFIM) by preparing thermofield double states at a variety of temperatures. We also prepare the critical state of the TFIM at zero temperature using quantum–classical hybrid optimization. The entanglement structure of thermofield double and critical states plays a key role in the study of black holes, and our work simulates such nontrivial structures on a quantum computer. Moreover, we find that the variational quantum circuits exhibit noise thresholds above which the lowest-depth QAOA circuits provide the best results.

quantum simulation | quantum computing | thermofield double state | Ising model | trapped ions

Progress in the control of synthetic quantum systems such as superconducting qubits (1) and trapped ions (2) has enabled continual advances in the depth of quantum computer circuits and the complexity of quantum simulations. As the number of qubits and their coherence times increase, such systems have the potential to simulate highly nontrivial macroscopic quantum phenomena. While there has been progress in the preparation of entangled quantum states such as squeezed or "cat" states (3, 4), much less attention has been paid to generating thermal (Gibbs) states of a many-body Hamiltonian, even though these states underpin phenomena ranging from high-temperature superconductivity (5) to quark confinement in quantum chromodynamics (6).

The simulation of many-body thermal states challenges currently available quantum platforms, owing to the required level of control over both the many-body interactions and the effective coupling to the thermal bath. Proposed schemes (7–9) to generate many-body thermal states involve subroutines like quantum-phase estimation, which are difficult to implement on near-term devices, or require engineered dissipative couplings (10). Experimental platforms such as optical lattices of ultracold atoms have enabled finite-temperature simulation (11, 12), but these are specific to particular (Hubbard) models, and cooling to low effective temperatures remains a major obstacle.

Here, we use an ion trap quantum computer to generate various nontrivial quantum states in the context of the many-body transverse-field Ising model (TFIM). We generate thermofield double (TFD) states (13), which are pure quantum states entangled between two systems, with the property that when either system is considered independently by tracing over the other, the TFD reduces to a thermal mixed state at a specified temperature. TFD states are purifications of thermal Gibbs states and have played a key role in the holographic correspondence relating a quantum-field theory to a gravitational theory in one higher dimension. In this correspondence, TFD states are dual to wormholes on the gravity side (14, 15) and enable teleportation ("traversable wormholes") (16, 17). The simulation of these concepts has motivated several approaches for preparing TFD states (18–21).

In this work, we use protocols (18) inspired by the alternation of unitary operators that forms the basis of the quantum approximate optimization algorithm (QAOA) (22). This scheme allows us to use unitary operations to control the effective temperature of a subsystem, thus foregoing the need of an external heat bath. We prepare TFD states of the quantum critical TFIM in a ring geometry composed of three trapped ion effective spins, at various target temperatures, as shown in Fig. 1. We also use a related approach (23) to directly prepare the zero-temperature ground state of the quantum critical TFIM with seven trapped ion spins using quantum–classical feedback.

TFD States

We briefly review the definition and preparation scheme of the TFD state. Consider two identical Hilbert spaces A and B consisting of qubits labeled by an index j. The Pauli spin operators on qubit j are labeled X_j, Y_j, and Z_j (24). Let H_A be a Hamiltonian with eigenstates $|n\rangle_A$ and corresponding energies E_n. A TFD state corresponding to inverse temperature β is defined on the joint systems A and B as

$$|TFD(\beta)\rangle = \frac{1}{\sqrt{Z(\beta)}} \sum_n e^{-\beta E_n/2} |n\rangle_A |n'\rangle_B , \qquad [1]$$

Significance

Our experiment prepares two types of nontrivial quantum states on a trapped ion quantum computer: the thermofield double state of the transverse-field Ising model at arbitrary temperature and the quantum critical state of the zero-temperature model. We use techniques motivated by the quantum approximate optimization algorithm, and we implement a hybrid quantum–classical optimization loop to prepare the quantum critical state. Our results pave the way for exploring strongly correlated models at finite temperature and teleportation protocols inspired by black hole physics.

Author contributions: D.Z., S.J., N.M.L., K.A.L., C.H.A., N.H.N., A.Y.M., T.H.H., and C.M. designed research, performed research, analyzed data, and wrote the paper.

Reviewers: D.H., Honeywell (United States); and M.S.-S., Stanford University.

Competing interest statement: C.M. is the cofounder and chief scientist at IonQ, Inc., a company that manufactures quantum computers. No IonQ employees, equipment, or other assets were involved with any aspect of the planning, design, execution, analysis, or reporting of this research.

[1]To whom correspondence may be addressed. Email: monroe@umd.edu.

This article contains supporting information online at https://www.pnas.org/lookup/suppl/doi:10.1073/pnas.2006337117/-/DCSupplemental.

First published September 28, 2020.

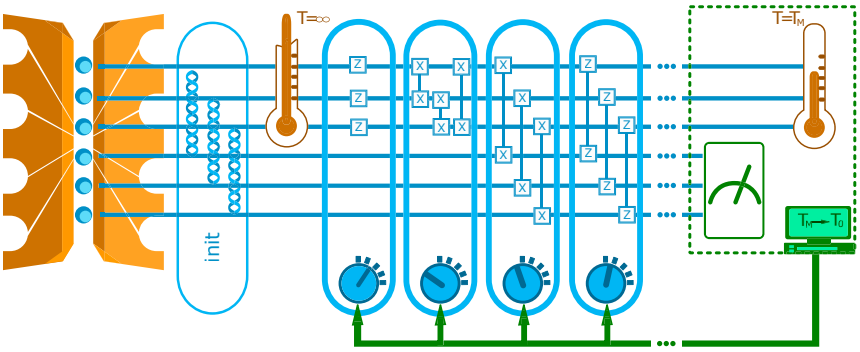

Fig. 1. Hybrid quantum–classical optimization circuit with trapped ion qubits to prepare thermal states. The initial Bell pairs (labeled init) denoted by ribbons connecting qubits 1 to 4, 2 to 5, and 3 to 6 (labeled 1 to 6 from top to bottom) correspond to the TFD state at infinite temperature. Layers of unitaries with independent control parameters are then applied sequentially to cool to the target temperature. The subsystem consisting of the first three qubits is effectively in the thermal (Gibbs) state. The result can be fed into a classical computer, which updates the parameters based on a cost function in a closed loop (*Full Hybrid Optimization: Preparation of Ground State of TFIM* has details).

where $Z(\beta)$ is a normalization factor. In general, the set $\{|n'\rangle_B\}$ can be any orthonormal basis spanning B, and we will make the choice $|n'\rangle = U|n\rangle$ where $U = \otimes_j Y_j$. This choice is consistent with the infinite-temperature TFD defined below. Tracing out the auxiliary system B results in the thermal (Gibbs) state of system A $\rho_A = e^{-\beta H_A}/Z(\beta)$; in this sense, realizing the TFD allows one to simulate the thermal Gibbs state in a subsystem A with the effective bath B.

The protocol (18) starts with an initial state $|\psi_0\rangle$ that is a product of Bell-pair singlets $\frac{1}{\sqrt{2}}(|0\rangle_A|1\rangle_B - |1\rangle_A|0\rangle_B)$ between pairs of A and B qubits. This is an infinite-temperature TFD since ρ_A is maximally mixed. Note that the two components of a Bell-pair singlet are related up to a phase by $Y|0\rangle = |1\rangle$ and $Y|1\rangle = -|0\rangle$, which justifies our choice of basis above. One then alternates between time evolution with the intersystem coupling $H_{AB} = \sum_i X_{i,A}X_{i,B} + Z_{i,A}Z_{i,B}$ and the intrasystem Hamiltonians $H_A + H_B$, where H_B is the rotated version of H_A ($UH_AU^\dagger$) acting on the B qubits. H_{AB} is chosen based on the fact that its ground state is $|\psi_0\rangle$, allowing for an adiabatic limit of our protocol described below. As in QAOA, each time step is a variational parameter, and after p layers of alternation, the resulting variational wave function is

$$|\psi(\vec{\alpha},\vec{\gamma})\rangle_p = \prod_{j=1}^{p} e^{i\alpha_j H_{AB}} e^{i\gamma_j (H_A+H_B)/2} |\psi_0\rangle . \qquad [2]$$

The variational parameters $\vec{\alpha},\vec{\gamma}$ are chosen to maximize the fidelity with the target TFD state: $F_p(\vec{\alpha},\vec{\gamma}) \equiv |\langle \mathrm{TFD}(\beta)|\psi(\vec{\alpha},\vec{\gamma})\rangle_p|^2$. As detailed in ref. 18, this protocol is guaranteed to target the zero-temperature TFD in the limit of large p because in that limit, it subsumes the adiabatic algorithm; the intuition, verified through several examples (18), is that the finite-temperature TFD is easier to prepare than zero-temperature ground state because the thermal correlation length is generally finite.

In the holographic correspondence, TFDs of conformal-field theories describing gapless quantum matter are particularly interesting because they correspond to wormholes on the gravity side. Their preparation is also useful to condensed matter physics because they enable investigation of finite-temperature properties of systems near a critical point by tracing over one of the systems in the double. Hence, our first objective is to prepare TFD states of the TFIM at its quantum critical point. Defined on a one-dimensional ring of L qubits, the TFIM Hamiltonian is

$$H_{TFIM} = \sum_{i=1}^{L} X_i X_{i+1} + g\sum_{i=1}^{L} Z_i \equiv H_{XX} + gH_Z . \qquad [3]$$

Here, g is the strength of the transverse field. When $g=1$, the ground state is a critical point between antiferromagnetic and paramagnetic quantum phases and has several interesting properties, including correlations between two spins decaying as a power of their separation and entanglement entropy scaling logarithmically with the size of the subsystem.

To prepare the TFD of the quantum critical TFIM, we tailor the general protocol above (Eq. **2**) to the capabilities of an experimental system with six trapped ions. The initial state is the product state of three spin-singlet Bell pairs formed between pairs of A and B spins. Ideally following the general protocol, we would like to evolve sequentially with $H_A = H_{XX} + H_Z$ (in addition to H_B), followed by

$$H_{AB} = \sum_i Z_{i,A}Z_{i,B} + \sum_i X_{i,A}X_{i,B} \equiv H_{ABZ} + H_{ABX} . \qquad [4]$$

Since H_{ABZ} and H_{ABX} commute, this step can be simply decomposed into evolution with each piece separately. However, time evolution with H_A in general requires a Trotter decomposition, which could require many steps beyond the capabilities of current experimental systems. Moreover, here H_B introduces additional gates, which we find are not essential for achieving high fidelity. In particular, in the $p=1$ ansatz, H_A and H_B act directly on the maximally entangled state $|\psi_0\rangle$, which has the property that $H_A|\psi_0\rangle = H_B|\psi_0\rangle$; thus, H_B is redundant in this case. Hence, we instead use a minimal variational ansatz for the TFD consisting of four pieces:

$$|\psi(\alpha_1,\alpha_2,\gamma_1,\gamma_2)\rangle = \exp(iH_{ABZ}\alpha_2)\exp(iH_{ABX}\alpha_1) \times \exp(iH_{XX}\gamma_2)\exp(iH_Z\gamma_1)|\psi_0\rangle . \qquad [5]$$

The first two operations represent a minimal Trotterization of time evolution with H_A. The optimal parameters are determined (on a classical computer) by maximizing the fidelity with the target TFD. In this case, the optimal fidelities are extremely good, ranging from 0.93 for the zero-temperature TFD to 1 for the infinite-temperature TFD. These can be further improved by adding additional iterations of this sequence of unitaries in the protocol. The single-body observables and two-point correlation functions of the optimized ansatz compare well with those of the target TFD, as evident in Fig. 2. We note that the general protocol preparing the TFD of the classical ($g=0$) Ising model achieves perfect fidelity for $p = L/2$ layers (18).

We experimentally run the optimized state-generation protocol on an ion trap quantum computer (*SI Appendix* has experimental details). To confirm the preparation of the TFD

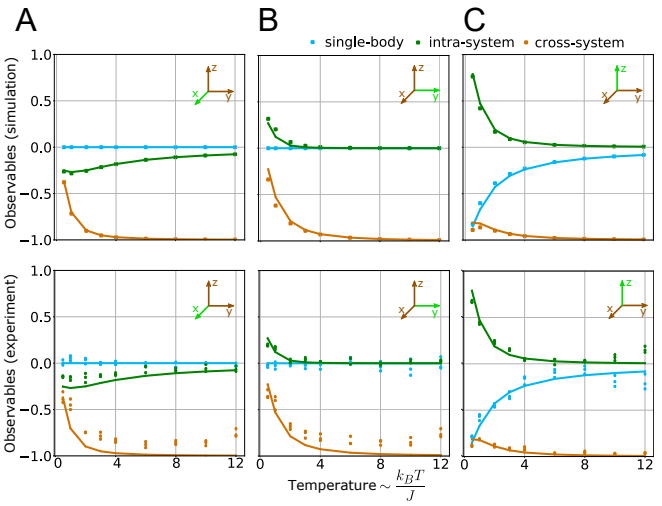

Fig. 2. Preparation of TFD states of the quantum critical TFIM using two 3-qubit systems. (*Upper*) Comparison between observables of the simulated optimized ansatz circuit and target TFD states (solid lines) for various target temperatures. (*Lower*) Comparison between observables of experimentally prepared and target TFD states. Results for all three ion pairs are given at each temperature. The measured correlation functions for different target temperatures are plotted against the theoretical expectations (solid lines) for type (*A*) Pauli-X, (*B*) Pauli-Y, and (*C*) Pauli-Z. Intrasystem correlators in subsystem *A* are $\langle\sigma_{1,A}\sigma_{2,A}\rangle$, $\langle\sigma_{1,A}\sigma_{3,A}\rangle$, and $\langle\sigma_{2,A}\sigma_{3,A}\rangle$. Cross-system correlators are $\langle\sigma_{1,A}\sigma_{1,B}\rangle$, $\langle\sigma_{2,A}\sigma_{2,B}\rangle$, and $\langle\sigma_{3,A}\sigma_{3,B}\rangle$. Note that the experimental data points in the figure have error bars accounting for statistical errors. Statistical error bars are similar in size or smaller than the symbols used. A symmetry-based error mitigation technique is used to post-process the experimental result in *C*. The mitigation notably improved the agreement between experiment and theory. Details are given in *SI Appendix*, Fig. S2.

state, we measure both intrasystem observables (single- and two-body correlation functions within system A) and intersystem correlators between corresponding sites from the A and B systems. The purpose of the intrasystem measurements is to verify physical properties of the thermal Gibbs state. In the phase diagram parameterized by temperature T and transverse field g, there is a regime $|g-1| << T << 1$ called the quantum critical fan (25), whose properties are dictated by the continuum theory of the critical point. For instance, this regime exhibits exponentially decaying correlations with correlation length proportional to inverse temperature in this case. Our intrasystem measurements could verify this phenomena and other features of the quantum critical fan for larger system sizes. The purpose of the intersystem measurements is to observe how correlations and entanglement between the two systems decrease as one lowers the target temperature and thereby, the thermal entropy (which in the TFD is the entanglement entropy between the systems).

As shown in Fig. 2, the results agree well with those expected from the TFD states, with some reduction in correlations caused by imperfect entangling operations. We note that at high temperature, there is a slight increase in error arising from an artifact of there being many sets of parameters that yield very good fidelities, and the optimal angles found are large enough to cause the observed errors (*SI Appendix*, Fig. S2). In fact, for such high temperatures, the initial set of Bell pairs is already a very good approximation to the target TFD, and it would be better to avoid using any gates.

Quantum Critical State at $T = 0$

To prepare the zero-temperature critical TFIM (pure) state, one does not require a purifying auxiliary system, and thus, a larger system A can be accessed experimentally. However, the long-range correlations and relatively high entanglement of the critical state pose challenges for preparation. Because a finite-depth circuit consisting of local gates can only produce a state with finite correlation length, to generate critical states one needs a quantum circuit (of local gates) with depth scaling with system size. With nonlocal gates, long-range correlated states can be prepared with fewer steps (26); however, tailoring the effective power law decaying interactions in trapped ion systems to target an arbitrary critical state is in general a difficult problem. One method for generating such critical states is the adiabatic algorithm, which requires tuning g adiabatically. On a digital quantum platform, this would require a compilation such as Trotterization into discrete gates, and the resulting deep circuit would be very susceptible to errors.

An alternative is the QAOA-motivated variational approach detailed in ref. 23. One begins with the product ground state of H_Z, which we denote $|0\rangle$, and then evolves with H_{XX}, H_Z in an alternating fashion:

$$|\psi(\vec{\alpha},\vec{\gamma})\rangle_p = e^{-i\alpha_p H_Z} e^{-i\gamma_p H_{XX}} \cdots e^{-i\alpha_1 H_Z} e^{-i\gamma_1 H_{XX}} |0\rangle . \quad [6]$$

Again, p denotes how many pairs of iterations are used, and in the hybrid quantum–classical optimization, $(\vec{\gamma},\vec{\beta})$ are variational parameters to be optimized to achieve the ground state of $-H_{XX} - H_Z$; in this section, we target the critical ground state of the ferromagnetic TFIM.

Trotterizing the adiabatic approach for preparing the critical state would lead to a unitary sequence of the above form, with $(\vec{\gamma},\vec{\beta})$ infinitesimal; this implies that for sufficiently large numbers of layers p, there is guaranteed to exist a set of parameters $(\vec{\gamma},\vec{\beta})$ for which the ansatz converges to the target state. However, the key question is how well the above ansatz performs for finite p. Remarkably, it has been observed that for a system size L, the above protocol can prepare the target critical state (and any state in the TFIM phase diagram) with perfect fidelity given $p = L/2$ layers (23).

For a trapped ion system of 7 qubits, a $p = 3$ protocol can generate the desired ground state with perfect fidelity, and we find the optimal angles $(\vec{\alpha},\vec{\gamma})$ on a classical computer to maximize the many-body overlap $|\langle\psi_t\ |\psi_p\rangle|^2$ of the ansatz $|\psi_p\rangle$ and the target state $|\psi_t\rangle$. While $p = 3$ layers exactly prepare the critical state, $p = 1, 2$ yield theoretical fidelities of 0.76 and 0.88, respectively.

For each number of layers p, we run the protocol with optimal angles on the trapped ion system and again measure two body correlation functions for Pauli-Z and Pauli-X operators (Fig. 3 *A* and *B*). The theoretical and experimental values agree well for the $p = 1$ protocol but deviate for $p = 2, 3$, as errors accumulate in the deeper circuit. The data show that larger p protocols are more effective at generating long-range correlation along the x direction but have more error in the Pauli-Z observable, resulting in less accurate energy. In particular, in the experiment the p = 3,2,1 protocols attain energies $-5.46 \pm -0.097, -7.74 \pm 0.095$, and -8.02 ± 0.043, respectively. In the simulation, the corresponding numbers are -8.98 for p = 3, -8.62 for p = 2, and -8.44 for p = 1. Fig. 4*A* provides a visual comparison. We find that the QAOA protocol with the least number of steps produces the state with the lowest energy, although theoretically, it should be the worst. This reflects the level of noise in the experimental system, which we discuss in the final section of this paper.

Full Hybrid Optimization: Preparation of Ground State of TFIM. Determining the optimal angles using classical simulation is feasible for current system sizes. For larger systems and higher p, however, one would need extrapolation based on patterns in the

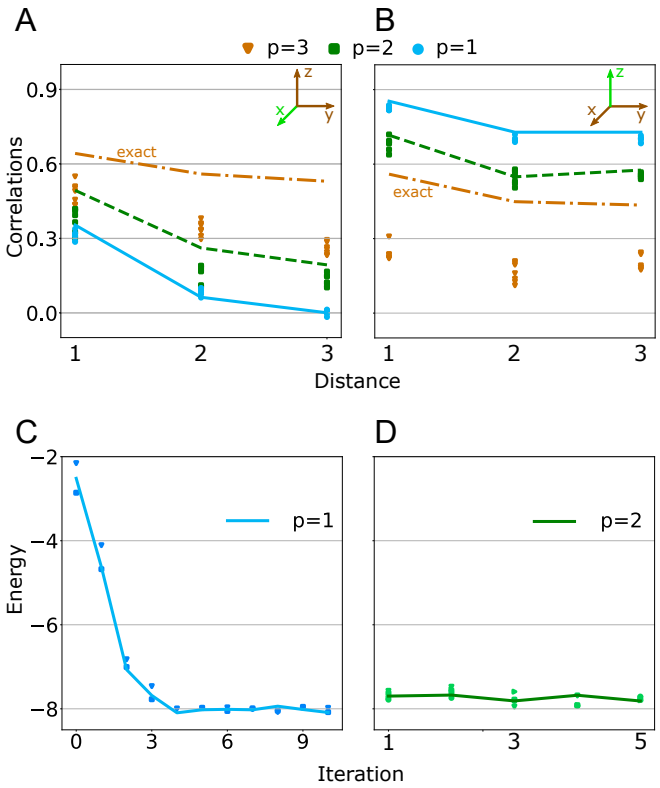

Fig. 3. Critical TFIM ground state on a 7-qubit system. (*A* and *B*) Two-point correlations for (*A*) Pauli-X and (*B*) Pauli-Z operators as a function of their separation. For a ring of seven spins, there are only three different pairs of ions, which are distinguishable by distance. The three different colors correspond to QAOA protocols with different depth p. The lines denote the theoretical expectations. (*C* and *D*) Energies achieved using full hybrid quantum–classical feedback with increasing gradient descent iteration number for (*C*) $p=1$, initialized with random parameter set, and (*D*) $p=2$, initialized with theoretically optimal parameters. The lines correspond to the measured energy at each iteration, and the dots correspond to samples taken to evaluate the gradients. Ideally, the lowest energy a $P=1$ protocol can reach is -8.44. The lowest energy a $P=2$ protocol can reach is -8.62. The true ground-state energy is -8.98, and the size of the gap is 0.23. The gap decreases linearly with system size. Statistical error bars in the figures are of the same size or smaller than the symbols used.

control parameters of QAOA protocols (27, 28). Therefore, a hybrid approach that involves a feedback loop between a quantum simulator and a classical computer has to be employed. As depicted in Fig. 1, one first carries out the unitary circuit for a given set of parameters and measures the energy cost function $E_p(\vec{\alpha},\vec{\gamma}) = {}_p\langle\psi(\vec{\alpha},\vec{\gamma})|-H_{XX}-H_Z|\psi(\vec{\alpha},\vec{\gamma})\rangle_p$. The lower the energy, the better this ansatz can approximate the critical ground state of $-H_{XX}-H_Z$. One then uses classical optimization to vary the parameters to lower the cost function until convergence is reached. One benefit of this hybrid scheme is that systematic errors from the quantum device are reduced.

We implement the full QAOA hybrid algorithm using standard gradient descent as the classical optimization strategy. To obtain an estimate of the partial derivatives, we change each parameter separately by a small amount and measure the corresponding energy difference. We then take a small (proportional to the gradient, with coefficient adjusted according to simulation) step along the gradient with all parameters. We target the critical TFIM ground state for $p=1$ starting from a random set of initial parameters. Results are shown in Fig. 3*C*. The optimization converges to a set of parameters that is different from the simulated result, but the measured energy matches the theoretical prediction for $p=1$.

To examine whether significant systematic errors play a role for deeper circuits in our experiment, we implement the hybrid optimization for $p=2$. This time, we initialize the process with the optimum values obtained from numerical simulation. A drop in the cost function would indicate that systematic errors shift the system away from the optimal state. The results in Fig. 3*D* show that this is not the case in our system.

Error Simulation. We simulate the QAOA protocol in the presence of noise for different numbers of layers p, analyzing the trade-off between theoretical and experimental errors. The 2-qubit XX gates are the main source of error in the experiment, likely limited by laser beam intensity fluctuation δI on the trapped ion qubits. Because the angle of the XX gate evolution depends on the square of the laser intensity I, the fractional error in the XX gate angle is $\Gamma = 2\delta I/I$. We model this error with a Monte Carlo simulation by setting the angle of the 2-qubit gate to be $\theta=\theta_0(1+\Gamma r)$, where θ_0 is the nominal gate angle and r is a Gaussian-distributed random number with mean 0 and SD 1, and we average over 1,000 samples. Fig. 4*A* shows the results for the variation of the measured energy vs. Γ. The three points marked in the figure indicate the experimentally measured values for the $p=1,2,3$ protocols. The value of the noise parameter Γ inferred from this error model is consistent between $p=2$ and $p=3$.

As seen in Fig. 4*A*, for $\Gamma \lesssim 0.13$, the higher-depth circuit produces a better outcome, and for higher levels of Γ, the lower-depth circuit is preferable. This implies a type of threshold noise behavior, where the optimization protocol converges to near-optimal solutions as long as the noise is below a critical value. The threshold can be explained by observing that the accuracy of QAOA for preparing ground states of Hamiltonians with unweighted terms is likely to increase exponentially with p (27), while the experimental accuracy on average decreases exponentially with p.

Generically, we also expect the 2-qubit gates to include some depolarizing error on the qubits involved in the gate. This error channel can be simulated by averaging over rotations ϕ around a random axis before every XX gate (*SI Appendix* has details). We parameterize the rotations by letting ϕ be a random variable with distribution $P(\phi)$ that is Gaussian with mean zero and SD λ. The variance in Γ is calculated for several values of λ between 0.1 and 0.3. Fig. 4 *B* and *C* shows results for different values of λ, with $\lambda=0.22$ being the point at which we can minimize the variance of the predicted Γ. This value corresponds to a 2-qubit depolarizing error of 2.37%. This agrees well with the typical experimentally

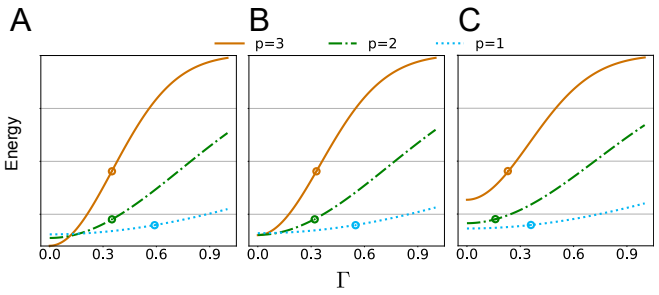

Fig. 4. Simulation results with noise for the $p=1,2,3$ QAOA protocols for preparation of the critical ground state of the TFIM. (*A*) $\lambda=0$ (no depolarizing noise), (*B*) $\lambda=0.1$, and (*C*) $\lambda=0.22$. Each curve is averaged over 1,000 samples. The circles in the figure show what Γ value an experimental result (shown in Fig. 3) predicts for a given set of p and λ. $\lambda=0.22$ is the point at which we can minimize the variance of the predicted Γ. Note that *A* shows a threshold at $\Gamma=0.13$, below which higher p gives better results.

PHYSICS

measured error rate of $1.5 \sim 2.5\%$, as described in *SI Appendix*. Note that the threshold for Γ described above appears for $\lambda < 0.1$, corresponding to a depolarizing error rate $< 0.5\%$.

Outlook

Our protocols for generating thermal states of qubits leverage the recent advent of variational approaches, in particular QAOA, and serve as the first step of several interesting directions. Even without the full hybrid quantum–classical scheme, our theoretical and experimental methods enable the exploration of very interesting physics. On one hand, the duality between a wormhole and a critical TFD can be taken one major step farther: the traversal of the wormhole corresponds to performing simple operations on the TFD state (16, 17). In experiment, this traversal could be confirmed by verifying teleportation between the two sides of the TFD. In a different vein, our critical TFIM ground-state preparation paves the way for extracting universal aspects of quantum criticality, such as the central charge of a conformal-field theory, from experiments. Additionally, one could use the TFD protocol to probe the quantum critical fan at finite temperature (25).

Our hybrid approach for creating pure ($T = 0$) states of the TFIM system also applies to thermal-state preparation. In that case, the cost function to be measured is the free energy on system A: $F_A = E_A - TS_A$, where $E_A = \mathrm{Tr}(\rho_A H_A)$ and $S_A = -\mathrm{Tr}(\rho_A \log \rho_A)$ are the energy and entanglement entropy between A and B, respectively. Estimating the latter would involve extrapolating from several Renyi entropy measurements, which requires either several copies of the system (29, 30) or randomized measurements on one copy (31). In the longer term, the hybrid approach for both quantum pure and thermal-state preparation may enable one to probe many-body physics on system sizes beyond the reach of classical computers and thus, shed light on the full (finite-temperature) phase diagram of intractable models.

On a practical level, our hybrid quantum–classical experiment and noise analysis suggest an error threshold that near-term devices must overcome to unlock the full potential of variational approaches.

Data Availability. All study data are included in the article and *SI Appendix*.

ACKNOWLEDGMENTS. We thank A. Seif for helpful discussions. This work is supported in part by the Army Research Office (ARO) through the Intelligence Advanced Research Programs Activity (IARPA) Logical Qubits program, the National Science Foundation Practical Fully-Connected Quantum Computer STAQ program, the Air Force Office of Scientific research Multi-University Research Initiative (MURI) programs on Quantum Measurement/Verification and Quantum Interactive Protocols, the ARO MURI on Modular Quantum Circuits, the Department of Energy (DOE) Basic Energy Sciences: Materials and Chemical Sciences for Quantum Information Science program DE-FOA-0001909 (optical design and instrumentation), the DOE High Energy Physics: Quantum Information Science Enabled Discovery program DE-FOA-0001893 (data analysis and interpretation), and the DOE Advanced Scientific Computing Research: Quantum Testbed program. Research at the Perimeter Institute is supported by the Government of Canada through Industry Canada and by the Province of Ontario through the Ministry of Research and Innovation. C.H.A. acknowledges financial support from the Mexican National Council of Science and Technology (CONACYT) Doctoral Grant 455378.

1. M. H. Devoret, R. J. Schoelkopf, Superconducting circuits for quantum information: An outlook. *Science* **339**, 1169–1174 (2013).
2. C. Monroe, J. Kim, Scaling the ion trap quantum processor. *Science* **339**, 1164–1169 (2013).
3. S. Haroche, Nobel lecture: Controlling photons in a box and exploring the quantum to classical boundary. *Rev. Mod. Phys.* **85**, 1083–1102 (2013).
4. O. Hosten, N. J. Engelsen, R. Krishnakumar, M. A. Kasevich, Measurement noise 100 times lower than the quantum-projection limit using entangled atoms. *Nature* **529**, 505–508 (2016).
5. P. A. Lee, N. Nagaosa, X. G. Wen, Doping a Mott insulator: Physics of high-temperature superconductivity. *Rev. Mod. Phys.* **78**, 17–85 (2004).
6. D. J. Gross, R. D. Pisarski, L. G. Yaffe, QCD and instantons at finite temperature. *Rev. Mod. Phys.* **53**, 43–80 (1981).
7. K. Temme, T. J. Osborne, K. G. Vollbrecht, D. Poulin, F. Verstraete, Quantum metropolis sampling. *Nature* **471**, 87–90 (2011).
8. B. M. Terhal, D. P. DiVincenzo, Problem of equilibration and the computation of correlation functions on a quantum computer. *Phys. Rev. A* **61**, 022301 (2000).
9. D. Poulin, P. Wocjan, Sampling from the thermal quantum Gibbs state and evaluating partition functions with a quantum computer. *Phys. Rev. Lett.* **103**, 220502 (2009).
10. F. G. S. L. Brandao, M. J. Kastoryano, Finite correlation length implies efficient preparation of quantum thermal states. arXiv:1609.07877v1 (26 September 2016).
11. R. Jördens, N. Strohmaier, K. Günter, H. Moritz, T. Esslinger, A Mott insulator of fermionic atoms in an optical lattice. *Nature* **455**, 204–207 (2008).
12. C. Gross, I. Bloch, Quantum simulations with ultracold atoms in optical lattices. *Science* **357**, 995–1001 (2017).
13. Y. Takahashi, H. Umezawa, Thermo field dynamics. *Int. J. Mod. Phys. B* **10**, 1755–1805 (1996).
14. W. Israel, Thermo-field dynamics of black holes. *Phys. Lett. A* **57**, 107–110 (1976).
15. J. Maldacena, Eternal black holes in anti-de sitter. *J. High Energy Phys.* **2003**, 021 (2003).
16. P. Gao, D. L. Jafferis, A. C. Wall, Traversable wormholes via a double trace deformation. *J. High Energy Phys.* **2017**, 151 (2017).
17. J. Maldacena, D. Stanford, Z. Yang, Diving into traversable wormholes. *Fortschr. Phys.* **65**, 1700034 (2017).
18. J. Wu, T. H. Hsieh, Variational thermal quantum simulation via thermofield double states. *Phys. Rev. Lett.* **123**, 220502 (2019).
19. J. Martyn, B. Swingle, Product spectrum ansatz and the simplicity of thermal states. *Phys. Rev. A* **100**, 032107 (2019).
20. W. Cottrell, B. Freivogel, D. M. Hofman, S. F. Lokhande, How to build the thermofield double state. *J. High Energy Phys.* **2019**, 58 (2019).
21. J. Maldacena, X.-L. Qi, Eternal traversable wormhole. arXiv:1804.00491v3 (15 October 2018).
22. E. Farhi, J. Goldstone, S. Gutmann, A quantum approximate optimization algorithm. arXiv:1411.4028 (14 November 2014).
23. W. W. Ho, T. H. Hsieh, Efficient variational simulation of non-trivial quantum states. *SciPost Phys.* **6**, 29 (2019).
24. M. A. Nielsen, I. L. Chuang, *Quantum Computation and Quantum Information* (Cambridge University Press, Cambridge, United Kingdom, 2000).
25. S. Sachdev, *Quantum Phase Transitions* (Cambridge University Press, 1999).
26. W. W. Ho, C. Jonay, T. H. Hsieh, Ultrafast variational simulation of nontrivial quantum states with long-range interactions. *Phys. Rev. A* **99**, 052332 (2019).
27. L. Zhou, S.-T. Wang, S. Choi, H. Pichler, M. D. Lukin, Quantum approximate optimization algorithm: Performance, mechanism, and implementation on near-term devices. *Phys. Rev. X* **10**, 021067 (2020).
28. F. G. S. L. Brandao, M. Broughton, E. Farhi, S. Gutmann, H. Neven, For fixed control parameters the quantum approximate optimization algorithm's objective function value concentrates for typical instances. arXiv:1812.04170 (11 December 2018).
29. S. Johri, D. S. Steiger, M. Troyer, Entanglement spectroscopy on a quantum computer. *Phys. Rev. B* **96**, 195136 (2017).
30. N. M. Linke *et al.*, Measuring the rényi entropy of a two-site fermi-Hubbard model on a trapped ion quantum computer. *Phys. Rev. A* **98**, 052334 (2018).
31. T. Brydges *et al.*, Probing Rényi entanglement entropy via randomized measurements. *Science* **364**, 260–263 (2019).